Article:
Ryder, CL, Highwood, EJ, Lai, TM et al. (2 more authors) (2013) Impact of atmospheric transport on the evolution of microphysical and optical properties of Saharan dust. Geophysical Research Letters, 40 (10). 2433 - 2438. ISSN 0094-8276

https://doi.org/10.1002/grl.50482

Impact of atmospheric transport on the evolution of microphysical and optical properties of Saharan dust

C. L. Ryder,[1] E. J. Highwood,[1] T. M. Lai,[2] H. Sodemann,[2] and J. H. Marsham[3]

Received 21 February 2013; revised 9 April 2013; accepted 15 April 2013; published 30 May 2013.

[1] Saharan dust affects the climate by altering the radiation balance and by depositing minerals to the Atlantic Ocean. Both are dependent on particle size. We present aircraft measurements comprising 42 profiles of size distribution (0.1–300 μm), representing freshly uplifted dust, regional aged dust, and dust in the Saharan Air Layer (SAL) over the Canary Islands. The mean effective diameter of dust in SAL profiles is 4.5 μm smaller than that in freshly uplifted dust, while the vertical structure changes from a low shallow layer (0–1.5 km) to a well-mixed deep Saharan dust layer (0–5 km). Size distributions show a loss of 60 to 90% of particles larger than 30 μm 12 h after uplift. The single scattering albedo (SSA) increases from 0.92 to 0.94 to 0.95 between fresh, aged, and SAL profiles: this is enough to alter heating rates by 26%. Some fresh dust close to the surface shows SSA as low as 0.85. **Citation:** Ryder, C. L., E. J. Highwood, T. M. Lai, H. Sodemann, and J. H. Marsham (2013), Impact of atmospheric transport on the evolution of microphysical and optical properties of Saharan dust, *Geophys. Res. Lett.*, *40*, 2433–2438, doi:10.1002/grl.50482.

1. Introduction

[2] During Northern Hemisphere summer, mineral dust over the Sahara is uplifted by strong surface winds, mixed vertically within the Saharan boundary layer (SABL), and typically transported westwards over the Atlantic Ocean in the Saharan Air Layer (SAL) [*Cuesta et al*., 2009; *Karyampudi et al*., 1999]. Dust laden air influences weather and climate by modifying the radiation balance, which can impact atmospheric circulation and surface temperatures over desert and ocean [*Evan et al*., 2008; *Highwood et al*., 2003; *Lavaysse et al*., 2011]. These radiative interactions are sensitive to dust size and optical properties [*Kok*, 2011; *McConnell et al*., 2010; *Otto et al*., 2009]. Additionally, the amount of soluble iron in ocean-deposited dust can be dependent on particle size [*Baker and Jickells*, 2006; *Ito et al*., 2012].

[3] Quantifying the impact of dust on the climate system depends on an accurate representation of any changes in dust properties during transport, which is a challenge for dust models [*Huneeus et al*., 2011]. Additionally, relatively few measurements are available for use in evaluating models which describe how dust properties depend on distance from source, particularly close to uplift time. Such measurements are needed to accurately model the impact on climate, and additionally to validate dust schemes in climate and numerical weather prediction models. Much recent work has explored the meteorological mechanisms behind dust uplift and transport over the Sahara, such as diurnal mixing of low-level jets to the surface and cold pool outflows from moist convection (haboobs) (as reviewed by *Knippertz and Todd* [2012]). However, accompanying work on the associated changes in dust microphysical and optical properties and their vertical distribution during these processes and particularly in subsequent transport has been sparse to date.

[4] *Maring et al*. [2003] examined change in dust size distribution with transport across the Atlantic Ocean, but the measurements in the Canary Islands and Puerto Rico were taken 5 years apart, and being ground-based were unable to provide vertically resolved measurements. *Weinzierl et al.* [2011] compared airborne dust size distributions between Morocco and Cape Verde, but measurements were taken during different years and seasons. Various aircraft measurements of dust over the eastern Atlantic have been made over the last 15 years [e.g., *Haywood et al*., 2011; *Haywood et al*., 2003; *McConnell et al*., 2008; *Otto et al*., 2007; *Weinzierl et al*., 2011] but repeated and consistent comparisons of dust profiles over ocean and desert are not available. Hence, *Prospero and Mayol-Bracero* [2012] and *Ansmann et al*. [2011] emphasize the need for an improved understanding of changes in dust properties during transport. Here we address this issue using new aircraft profile measurements at different stages of the dust lifecycle over Africa and the Eastern Atlantic.

2. Method

2.1. Measurement Locations and Flights

[5] As part of the Fennec project [*Marsham et al*., 2013; *Washington et al*., 2012], the UK's BAe-146-301 Research Aircraft operated by the Facility for Airborne Atmospheric Measurements was stationed at Fuerteventura, Canary Islands from 17 to 28 June 2011. During missions conducted over the Sahara Aerosol Optical Depths (AODs), up to 3.1 (at 550 nm, calculated from airborne scattering and absorption measurements) were measured [*Ryder et al*., 2013]. During the same time period, two Saharan dust outbreaks over the Canary Islands occurred with AODs up to 1.1. As a consequence, the aircraft sampled the vertical profile of dust over both the Sahara (Mauritania and Mali) and the

Additional supporting information may be found in the online version of this article.

[1]Department of Meteorology, University of Reading, Reading, UK.
[2]Institute for Atmospheric and Climate Science, ETH Zurich, Zürich, Switzerland.
[3]School of Earth and Environment, University of Leeds, Leeds, UK.

Corresponding author: C. L. Ryder, Department of Meteorology, University of Reading, Earley Gate, Reading, RG6 6BB, UK. (c.l.ryder@reading.ac.uk)

0094-8276/13/10.1002/grl.50482

eastern Atlantic Ocean, between the African coast and Fuerteventura, through ascents and descents as part of the flight track. In total, 42 profiles were performed (see supporting information for full details and flight tracks). Over ocean, profiles were sampled from the surface to cruising altitude (around 8 km), whereas over the desert, the aircraft minimum altitude varied between 100 m to 1 km above ground level.

2.2. Instrumentation

[6] The aircraft was extensively equipped to measure properties of Saharan dust. Data presented here were measured by using a Passive Cavity Aerosol Spectrometer Probe (PCASP, 0.13–3.5 μm, accumulation mode), a Cloud Droplet Probe (CDP, 2.9–44.6 μm, coarse mode), and a Cloud Imaging Probe (CIP, 37.5–300 μm, giant mode). Diameters measured by the PCASP and CDP have been corrected for a refractive index appropriate for dust (1.53–0.001i) and for instrumental drift during the campaign. Subsequent agreement between different instrumental size ranges is excellent [see *Ryder et al*., 2013 for further details]. Size ranges for each instrument are slightly different to the full size range available and are selected here to provide a complete but not overlapping size distribution of the mid points of the size bins, which results in the bin edges overlapping slightly. Henceforth, all size measurements refer to diameter (d).

[7] The aircraft performs scientific profiles at vertical velocities of around 5 ms^{-1} and horizontal velocities of 110 ms^{-1}, resulting in a slanted vertical profile typically covering around 170 km horizontally, which is smaller than the scale of dust events sampled. Data have been merged onto a 50 m vertical grid to reduce the variability and make visualization clearer. Optical properties are calculated from size distributions on the 50 m grid using a Mie scattering code. For simplicity we make the assumption of a refractive index of 1.53–0.001i, which is constant with particle size and spherical particles, both of which may vary in reality [e.g., *Kandler et al*., 2011] The single scattering albedo is particularly sensitive to choice of refractive index. We solely present data regarding size distributions; chemical composition and particle shape are not included in the analysis. Locations are selected where number concentrations were larger than 10 cm^{-3} to ensure dust was present, and measurements within clouds were excluded based on relative humidity and particle number concentrations recorded by the CDP.

2.3. Categorization of Profiles

[8] We separate profile measurements into three categories: fresh, aged, and SAL (i.e., transported over the adjacent east Atlantic). The dust sampled over desert consisted of a mixture of cases from very freshly uplifted dust, to dust several days old, which had originated from Mali and Algeria. *Ryder et al*. [2013] examined measurements from horizontal flight legs, calculating dust age based on Spinning Enhanced Visible and Infrared Imager (SEVIRI) RGB 15 min resolution satellite imagery and HYSPLIT back trajectories [*Draxler and Hess*, 1998]. Here we use profile measurements which correspond to the same cases. We combine the two fresh categories of *Ryder et al*. [2013] into a single "fresh desert" category, consisting of five profiles, representing dust uplifted within 12 h prior to measurement. We combine all other profiles measured over desert into an "aged desert" category (15 profiles), where dust has been mobilized 12 to 70 h prior to measurement, with sources in central and eastern Algeria, and in central north Mali for one case (flight b604).

[9] We use 21 profile measurements in the region of Fuerteventura to construct a typical "SAL" category. The likely source locations and age of the SAL profiles have been estimated using Lagrangian backward calculations with the FLEXPART model [*Stohl et al*., 2005]. Dust uplift potential [*Marsham et al*., 2011] is calculated along 7 day kinematic back-trajectories when the air mass was within the boundary layer, using European Centre Medium Range Weather Forecast meteorological analysis data. This provides an insight into both times and locations when surface winds were strong enough for dust uplift [*Sodemann et al*., 2006]. The results indicate that the SAL dust was at least 18 h old, with a mean and median "age" of 87 and 77 h, respectively. Likely sources were mainly over Western Sahara, northern Mauritania, and eastern and central Algeria. Additional assessments using SEVIRI images and HYSPLIT back trajectories implied similar dust uplift locations and ages. Thus, it seems that the dust measured over the ocean probably had largely similar source locations as the desert measurements, (although from forward calculations (not shown), we cannot confirm direct Lagrangian transport of dust sampled over the desert to the SAL profiles).

3. Results

3.1. Size Distributions

[10] In Figure 1, a decrease in number concentration at all altitudes and at all particle sizes is evident—first, from fresh to aged, and second, a further decrease from aged dust to SAL (excluding the marine boundary layer (MBL), beneath 1 km in SAL profiles, which is not considered here). Small number concentrations of giant particles ($d > 37.5$ μm) are present beneath 3 km in the fresh desert category (Figure 1c). These are no longer present in the aged desert category except for a narrow peak at around 500 m. This peak is entirely caused by a contribution from one individual profile (flight b604) when a geographically large dust event originating from a mesoscale convective system in Mali was transported over Mauritania. Therefore, although giant mode particles do not generally appear to be transported for longer time scales than 12 h, it is possible in very large dust events. For SAL profiles, giant particles are absent.

[11] For fresh desert cases, a decrease in number concentration with altitude at all particle size ranges is evident, particularly beneath 2 km. This is consistent with freshly uplifted dust at the surface being mixed through the convective boundary layer (CBL), during the morning break down of the low-level jet (LLJ, *Marsham et al*. [2013]). As the dust ages, it is mixed vertically upwards through the deep SABL, and vertical profiles become much more constant for the aged desert category (green lines in Figures 1a and 1b), and also the SAL profiles (blue lines).

[12] Figure 1d shows effective diameter (d_{eff}) of the full size distribution as a function of altitude. d_{eff} is largest for the fresh desert cases, particularly at the lowest altitudes with a mean and 90th percentile value of 13.2 and 25.2 μm, respectively. Second, a decrease in d_{eff} is observed between the fresh desert and aged desert cases, and again

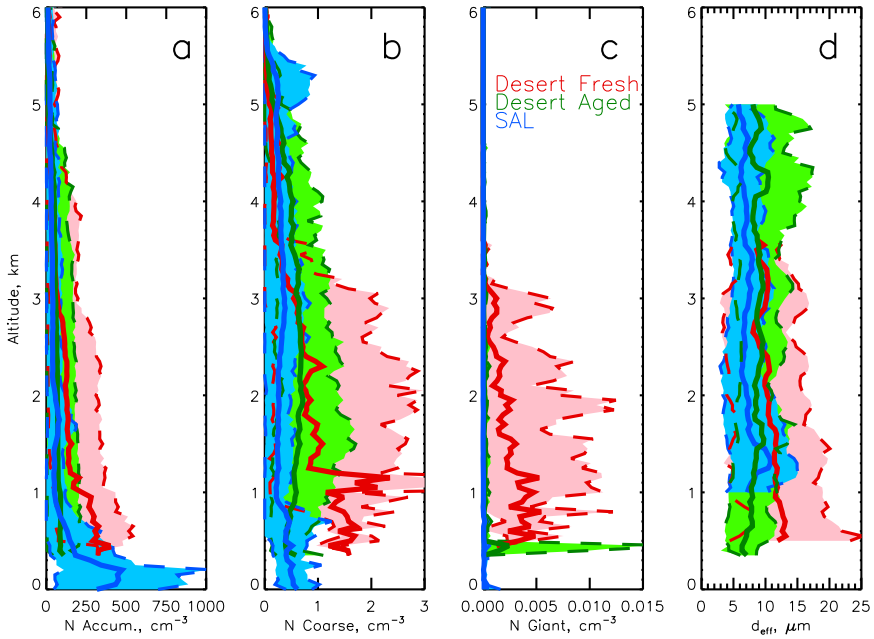

Figure 1. (a–c) Number concentrations and (d) effective diameter for fresh desert (red), aged desert (green), and SAL (blue) categories as a function of measurement altitude. Solid lines show means, dashed lines and shading indicate 10th and 90th percentiles, respectively. Number concentrations are depicted by totals for each part of the size distribution covering diameters of 0.13–3.5 µm (accumulation mode), 2.9–44.6 µm (coarse mode), and 37.5–300 µm (giant mode). Desert data in Figures 1a–1c does not extend to the surface as the aircraft did not land over the desert. In Figure 1d SAL profile MBL data is omitted, and desert data is shown only where at least three profile measurements are available.

from the aged desert to SAL cases. Column mean values (10th and 90th percentiles) of d_{eff} decrease from 10.6 (4.7 to 16.8) µm for fresh desert cases, to 8.6 (5.2 to 12.9) µm for aged desert profiles, to 7.2 (4.1 to 10.7) µm for SAL profiles. The decrease in d_{eff} during transport suggests a preferential loss of the larger particles with respect to the smaller ones.

[13] While d_{eff} decreases with altitude for the fresh cases, it is relatively constant with altitude for the aged desert and SAL cases, by which time the dust is well mixed within the deep SABL or the SAL. This is also reflected in the volume size distributions (Figure in supporting information)—fresh desert cases show a decreasing total concentration and contribution of giant particles with altitude whereas aged and SAL profiles show sharp decreases in concentrations at 5 km (the top of the SABL and SAL).

3.2. Particle Loss During Transport

[14] Figure 2a shows the column-mean normalized volume size distributions. The measurements show a loss of particles between 0.4 to 200 µm in the transition from fresh, to aged, to SAL profiles, and a loss of the giant mode, especially for SAL cases.

[15] Figure 2b shows the fractional change in the normalized number size distributions (i.e., divided by total number concentration), between fresh desert and aged desert categories (red), and between aged desert and SAL categories (green), after *Maring et al*. [2003]. Fairly constant losses of around 20 to 40% of particles sized between 0.4 to 20 µm for both transitions (red and green lines) are shown, with some variations between the two stages, although they do not emerge outside the error bars. At sizes larger than 20 µm, there is an increase in fractional loss for both lines, consistent with preferential deposition of the largest particles. Between 60 and 90% of particles sized between 30 and 200 µm are lost between fresh and aged desert profiles, i.e., subsequent to 12 h after uplift. One hundred percent of these particles are absent in the SAL profile column mean. Note that the column-mean size distribution over the ocean still has a relatively large coarse mode, with a peak normalized volume size distribution at 10 to 20 µm.

[16] Contrastingly, *Maring et al*. [2003] found a preferential loss of particles larger than 7.3 µm across the Atlantic from surface measurements. We report fractional losses of 20 to 40% between 4 to 30 µm, whereas losses of *Maring et al*. [2003] were closer to zero. *Weinzierl et al*. [2011] compared dust measurements from different years over Morocco to the Atlantic Ocean, finding that over land particles sized larger than 40 µm were present 20% of the time compared to 0% over the ocean. Results presented here show that the recently observed number concentrations of very large dust particles over the Sahara during the Fennec project [*Ryder et al*., 2013] are not observed over ocean when probed with the same instrumentation. Clearly, dust size distribution changes very rapidly following dust uplift and close to the African coast.

3.3. Mechanisms for Size Distribution Change

[17] Applying settling velocities from *Li and Osada* [2007] in the absence of turbulence, giant mode particles would fall the 5 km SABL depth within 12.5 ± 4 h. This explains the loss of giant particles between the fresh and aged profiles (Figure 1c) in all cases, except for flight b604 where giant particles were transported over longer time scales, perhaps due to overnight turbulence in cold-pool outflow. Deposition also plays a role for coarse mode

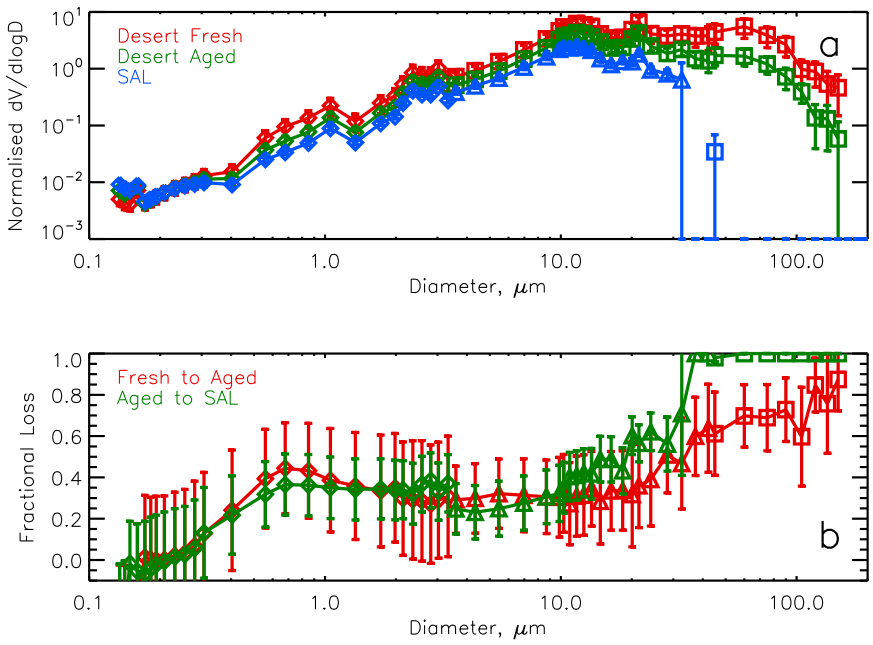

Figure 2. (a) Column mean normalized size distributions fresh desert (red, beneath 5.5 km), aged desert (green), and SAL (blue, between 1.5 and 5.5 km representing the SAL). (b) Normalized fractional loss in number size distribution between fresh desert and aged desert (red) and aged desert to SAL (green). Error bars represent standard errors.

particles, which fall the same distance over any time from 20 ± 5 h (d = 30 μm) to several days (d = 4 μm). Despite this, coarse mode particles are not completely depleted by either the aged or SAL categories. Accumulation mode particles (d < 3.5 μm, to coincide with PCASP measurements) are deposited on a time scale lasting tens of days or more, suggesting a lesser role for deposition, even for the Eastern Atlantic SAL profiles.

[18] In addition to deposition, particles are also subject to a decrease in concentration via dispersion. According to Gaussian plume theory, plume area will increase proportionally to time if the lower and upper edges are bounded by the ground surface and a temperature inversion at the top of the SABL [*Dacre et al.*, 2013]. Therefore, for the transition from aged to SAL, mean time scales are 40 to 80 h, so number concentrations could be expected to

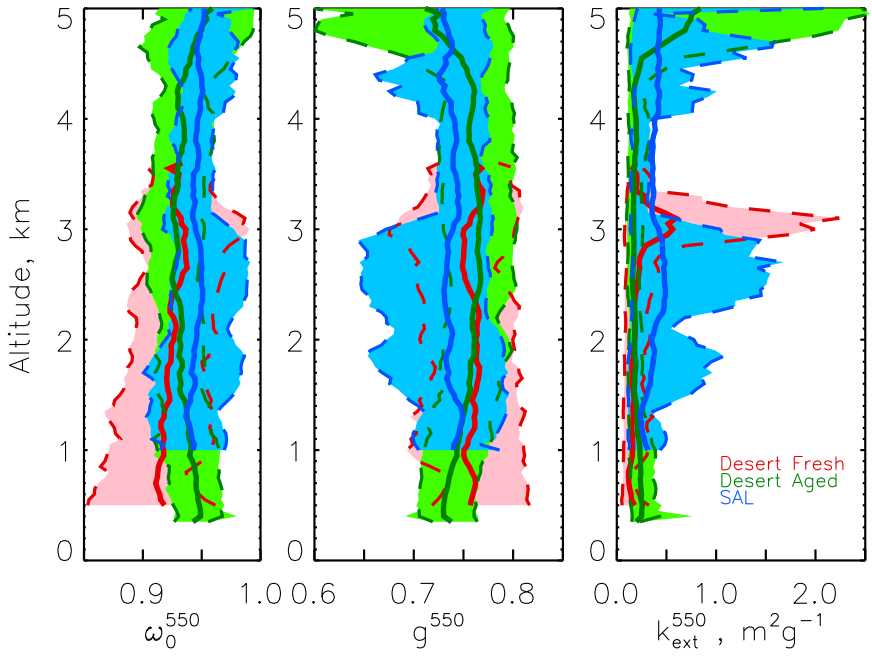

Figure 3. Optical properties ((a) SSA, (b) g, (c) k_{ext}, all at 550 nm) calculated from size distributions, for fresh desert (red), aged desert (green), and SAL (blue) categories as a function of measurement altitude. Solid lines show means, dashed lines and shading indicate 10th and 90th percentiles, respectively. Ocean (blue) lines are not shown beneath 1 km due to boundary layer contamination of non-dust aerosols, and desert data is not shown where fewer than three profiles are present.

decrease by a factor of 2. Measurements between aged and SAL categories decrease by around a factor of 2 and 1.3 for accumulation and coarse modes, respectively, on an order of magnitude in agreement with dispersion theory: the greater loss of accumulation compared with coarse mode is at odds with the greater loss of coarse mode expected from deposition and may result from the lack of an exact Lagrangian match. Dispersion between fresh and aged categories is more difficult to evaluate since source strength varies between dust events (and was not measured), and the dust plume is still being mixed vertically throughout the SABL at this stage.

3.4. Optical Properties

[19] We now present the changes in optical properties that result from the size changes during transport. Figures 3a–3c show the vertical profiles of mean (solid lines), 10th and 90th percentiles (dashed lines and shading) of the optical properties against altitude over land and ocean, calculated from Mie scattering using the measured size distributions, for single scattering albedo (SSA), asymmetry parameter (g) and mass specific extinction (k_{ext}), at 550 nm.

[20] All the parameters shown in Figure 3 respond to the decrease in d_{eff} between fresh desert, aged desert, and SAL categories, with an increase in SSA and k_{ext}, and a decrease in g (see also Figure in supporting information). This results from the smaller SAL particles being less absorbing, having higher extinction properties per unit mass, and being less forward scattering. Changes between the fresh and aged desert categories are particularly noticeable at low altitudes where the largest particles are present in fresh cases. The column mean beneath 1.5 km changes from 0.92 to 0.94 for SSA, 0.76 to 0.74 for g, and 0.15 to 0.23 m^2g^{-1} for k_{ext}, from fresh to aged. For a constant AOD of 1.0, these changes would decrease the instantaneous solar heating rate by 26%. Changes in optical properties at higher altitudes between fresh and aged desert are not obvious due to the similar d_{eff} values shown in Figure 1d.

[21] Changes are also observed between aged desert and SAL categories, with changes in the column mean from 0.94 to 0.95 for SSA, 0.75 to 0.74 for g and 0.23 to 0.39 m^2g^{-1} for k_{ext}, consistent with further losses of coarse and giant particles. This would result in a decreased instantaneous solar heating rate of 17%.

4. Conclusions

[22] We have presented vertically resolved aircraft measurements of Saharan dust over remote desert (fresh and aged cases) and the Atlantic Ocean, to compare quantitatively the dust properties during various stages in its life cycle. We have used consistent instrumentation for size distribution measurements from 0.1 to 300 μm diameter, larger than has previously been measured for airborne Saharan dust measurements.

[23] Vertical profiles of number concentration for the fresh desert dust reveal that dust is initially present in a shallow layer during the morning following uplift by low-level jets and cold pools, with high concentrations of coarse and giant mode present. Above 3 km, number concentration and the contribution from giant and coarse mode sizes decreases rapidly. During the day (and subsequent days), dust is mixed throughout the deep SABL by dry convection up to 5–6 km, becoming well-mixed vertically and losing a substantial fraction of the giant mode in most cases, after 12 h subsequent to uplift (60–90% of particles larger than 30 μm were not present in cases older than 12 h). One large haboob, however, did retain significant giant mode particles beyond 12 h, suggesting that such events should not be precluded from containing the largest particles over continental-scale transport distances. In comparison to the fresh desert cases, the aged desert category had a lower column mean d_{eff} of 8.1 μm and higher SSA of 0.94 beneath 1.5 km, enough to decrease instantaneous solar heating rates by 26%.

[24] The transition from aged desert to SAL profiles demonstrated further aging of the dust, with the mean column size distributions showing 100% loss of particles larger than 30 μm by the time the air reached the Canary Islands. Although the coarse mode was still present over ocean, the proportional volume of the size distribution it contained was reduced. The vertical distribution of dust remained relatively constant throughout the SAL, as expected, with strong similarities to the aged desert category, although with the development of a MBL beneath the SAL. Column-mean size distributions demonstrate preferential loss at sizes greater than 30 μm during transport, as might be expected close to active dust sources.

[25] Changes over the time scales examined here are consistent with deposition theory (loss of the giant mode after 12 h' transport), and dispersion theory (decreases in concentration of the accumulation mode between aged and SAL profiles). However, neither are able to explain retention of the coarse mode particles, which is greater than expected from deposition, similar to *Maring et al*. [2003], who found that Stokes velocities alone were not able to explain measured size distributions. It is possible that other mechanisms play a role, such as buoyancy and/or turbulence in the SABL and SAL, or electrostatic charging of particles (e.g., *Nicoll et al*. [2011]), or that the lack of direct Lagrangian transport here influenced the results.

[26] Rapid changes in number concentration, size distribution, and optical properties, as shown here, are important for mineral deposition to the Atlantic Ocean and the radiative effect of dust. Thus, it is a challenge to models which include dust to accurately model these changes during transport. Given the dependence of optical properties on size, and the estimated changes of 26% in solar heating rate simply due to SSA changes, studies examining the radiative impact of dust on circulation should use appropriately varying size distributions and dust optical properties. This could be achieved by interactive optical property calculations linked to improved modeled size distribution and evaluated using measurements such as those presented in this study, or at least by using a different radiative description of dust close to the source.

[27] **Acknowledgments.** Project funding for Fennec was from UK NERC grant NE/G017166/. Airborne data was obtained using the BAe-146-301 Atmospheric Research Aircraft operated by Directflight Ltd and managed by FAAM. The authors acknowledge the dedicated work of FAAM, Directflight, Avalon, and mission scientists during the Fennec 2011 aircraft campaign. H. Dacre is thanked for insightful comments regarding atmospheric dispersion. EUFAR is acknowledged for funding through the Transnational Access project LADUNEX (H.S.) and through their Education and Training program (T.M.L.).

[28] The Editor thanks Bernadett Weinzierl and an anonymous reviewer for their assistance in evaluating this paper.

References

Ansmann, A., A. Petzold, K. Kandler, I. Tegen, M. Wendisch, D. Müller, B. Weinzierl, T. Müller, and J. Heintzenberg (2011), Saharan mineral dust experiments SAMUM-1 and SAMUM-2: What have we learned?, *Tellus B*, *63*(4), 403–429.

Baker, A. R., and T. D. Jickells (2006), Mineral particle size as a control on aerosol iron solubility, *Geophys. Res. Lett.*, *33*, L17608, doi:10.1029/2006GL026557.

Cuesta, J., J. H. Marsham, D. J. Parker, and C. Flamant (2009), Dynamical mechanisms controlling the vertical redistribution of dust and the thermodynamic structure of the West Saharan atmospheric boundary layer during summer, *Atmos. Sci. Lett.*, *10*(1), 34–42.

Dacre, H. F., A. L. M. Grant, and B. T. Johnson (2013), Aircraft observations and model simulations of concentration and particle size distribution in the Eyjafjallajokull volcanic ash cloud, *Atmos. Chem. Phys.*, *13*, 1277–1291.

Draxler, R. R., and G. D. Hess (1998), An overview of the HYSPLIT_4 modeling system of trajectories, dispersion, and deposition, *Aust. Meteor. Mag.*, *47*, 295–308.

Evan, A. T., A. K. Heidinger, R. Bennartz, V. Bennington, N. M. Mahowald, H. Corrada-Bravo, C. S. Velden, G. Myhre, and J. P. Kossin (2008), Ocean temperature forcing by aerosols across the Atlantic tropical cyclone development region, *Geochem. Geophys. Geosyst.*, *9*.

Haywood, J. M., P. Francis, S. Osborne, M. Glew, N. Loeb, E. Highwood, D. Tanre, G. Myhre, P. Formenti, and E. Hirst (2003), Radiative properties and direct radiative effect of Saharan dust measured by the C-130 aircraft during SHADE: 1. Solar spectrum, *J. Geophys. Res.*, *108*(D18), 8577, doi:10.1029/2002JD002687.

Haywood, J. M., B. T. Johnson, S. R. Osborne, J. Mulcahy, M. E. Brooks, M. A. J. Harrison, S. F. Milton, and H. E. Brindley (2011), Observations and modelling of the solar and terrestrial radiative effects of Saharan dust: A radiative closure case-study over oceans during the GERBILS campaign, *Q. J. R. Meteorol. Soc.*, *137*(658), 1211–1226.

Highwood, E. J., J. M. Haywood, M. D. Silverstone, S. M. Newman, and J. P. Taylor (2003), Radiative properties and direct effect of Saharan dust measured by the C-130 aircraft during Saharan Dust Experiment (SHADE): 2. Terrestrial spectrum, *J. Geophys. Res.*, *108*(D18), 8578, doi:10.1029/2002JD002552.

Huneeus, N. et al. (2011), Global dust model intercomparison in AeroCom phase I, *Atmos Chem Phys*, *11*(15), 7781–7816.

Ito, A., J. Kok, Y. Feng, and J. Penner (2012), Does a theoretical estimation of the dust size distribution at emission suggest more bioavailable iron deposition?, *Geophys. Res. Lett.*, *39*(L05807), doi:10.1029/2011GL050455.

Kandler, K. et al. (2011), Electron microscopy of particles collected at Praia, Cape Verde, during the Saharan Mineral Dust Experiment: particle chemistry, shape, mixing state and complex refractive index, *Tellus B*, *63*(4), 475–496.

Karyampudi, V. M. et al. (1999), Validation of the Saharan dust plume conceptual model using lidar, Meteosat, and ECMWF data, *Bull. Am. Meteorol. Soc.*, *80*(6), 1045–1075.

Knippertz, P., and M. C. Todd (2012), Mineral dust aerosols over the Sahara: meteorological controls on emission and transport and implications for modeling, *Rev. Geophys.*, *50*, RG1007, doi:10.1029/2011RG000362.

Kok, J. F. (2011), A scaling theory for the size distribution of emitted dust aerosols suggests climate models underestimate the size of the global dust cycle, *Proc. Natl. Acad. Sci. U. S. A.*, *108*(3), 1016–1021.

Lavaysse, C., J. P. Chaboureau, and C. Flamant (2011), Dust impact on the West African heat low in summertime, *Q. J. R. Meteorol. Soc.*, *137*(658), 1227–1240.

Li, J. M., and K. Z. Osada (2007), Preferential settling of elongated mineral dust particles in the atmosphere, *Geophys. Res. Lett.*, *34*, L17807, doi:10.1029/2007GL030262.

Maring, H., D. L. Savoie, M. A. Izaguirre, L. Custals, and J. S. Reid (2003), Mineral dust aerosol size distribution change during atmospheric transport, *J. Geophys. Res.*, *108*(D19), 8592, doi:10.1029/2002JD002536.

Marsham, J. H., P. Knippertz, N. S. Dixon, D. J. Parker, and G. M. S. Lister (2011), The importance of the representation of deep convection for modeled dust-generating winds over West Africa during summer, *Geophys. Res. Lett.*, *38*, L16803, doi:10.1029/2011GL048368.

Marsham, J. H. et al. (2013), Meteorology and dust in the central Sahara: Observations from Fennec superiste-1 during the June 2011 Intensive Observation Period, *J. Geophys. Res.*, doi:10.1002/jgrd.50211.

McConnell, C. L., E. J. Highwood, H. Coe, P. Formenti, B. Anderson, S. Osborne, S. Nava, K. Desboeufs, G. Chen, and M. A. J. Harrison (2008), Seasonal variations of the physical and optical characteristics of Saharan dust: Results from the dust outflow and deposition to the ocean (DODO) experiment, *J. Geophys. Res.*, *113*, D14S05, doi:10.1029/2007JD009606.

McConnell, C. L., P. Formenti, E. J. Highwood, and M. A. J. Harrison (2010), Using aircraft measurements to determine the refractive index of Saharan dust during the DODO Experiments, *Atmos. Chem. Phys.*, *10*(6), 3081–3098.

Nicoll, K. A., R. G. Harrison, and Z. Ulanowski (2011), Observations of Saharan dust layer electrification, *Environ. Res. Lett.*, *6*(1).

Otto, S., M. de Reus, T. Trautmann, A. Thomas, M. Wendisch, and S. Borrmann (2007), Atmospheric radiative effects of an in situ measured Saharan dust plume and the role of large particles, *Atmos. Chem. Phys.*, *7*(18), 4887–4903.

Otto, S., E. Bierwirth, B. Weinzierl, K. Kandler, M. Esselborn, M. Tesche, A. Schladitz, M. Wendisch, and T. Trautmann (2009), Solar radiative effects of a Saharan dust plume observed during SAMUM assuming spheroidal model particles, *Tellus B*, *61*(1), 270–296.

Prospero, J. M., and O. L. Mayol-Bracero (2012), Improving our understanding of African dust transport using the Caribbean Basin as the receptor, in *IGAC Newsletter*, edited, pp. 10–14.

Ryder, C. L. et al. (2013), Optical properties of Saharan dust aerosol and contribution from the coarse mode as measured during the Fennec 2011 aircraft campaign, *Atmos. Chem. Phys.*, *13*, 303–325.

Sodemann, H., A. S. Palmer, C. Schwierz, M. Schwikowski, and H. Wernli (2006), The transport history of two Saharan dust events archived in an Alpine ice core, *Atmos. Chem. Phys.*, *6*, 667–688.

Stohl, A., C. Forster, A. Frank, P. Seibert, and G. Wotawa (2005), Technical note: The Lagrangian particle dispersion model FLEXPART version 6.2, *Atmos. Chem. Phys.*, *5*, 2461–2474.

Washington, R. et al. (2012), Fennec—The Saharan climate system, *CLIVAR Exchanges*, *17*(60), 31–32.

Weinzierl, B. et al. (2011), Microphysical and optical properties of dust and tropical biomass burning aerosol layers in the Cape Verde region-an overview of the airborne in situ and lidar measurements during SAMUM-2, *Tellus B*, *63*(4), 589–618.